First-principles study of tunneling magnetoresistance in $Fe/MgAl_2O_4/Fe(001)$ magnetic tunnel junctions

Yoshio Miura,* Shingo Muramoto, Kazutaka Abe, and Masafumi Shirai
Research Institute of Electrical Communication (RIEC) and Center for Spintronics Integrated Systems (CSIS), Tohoku University, Katahira 2-1-1, Aoba-ku, Sendai 980-8577, Japan
(Received 1 March 2012; revised manuscript received 18 June 2012; published 20 July 2012)

We investigated the spin-dependent transport properties of $Fe/MgAl_2O_4/Fe(001)$ magnetic tunneling junctions (MTJs) on the basis of first-principles calculations of the electronic structures and the ballistic conductance. The calculated tunneling magnetoresistance (TMR) ratio of a $Fe/MgAl_2O_4/Fe(001)$ MTJ was about 160%, which was much smaller than that of a Fe/MgO/Fe(001) MTJ (1600%) for the same barrier thickness. However, there was an evanescent state with Δ_1 symmetry in the energy gap around the Fermi level of normal spinel $MgAl_2O_4$, indicating the possibility of a large TMR in $Fe/MgAl_2O_4/Fe(001)$ MTJs. The small TMR ratio of the $Fe/MgAl_2O_4/Fe(001)$ MTJ was due to new conductive channels in the minority spin states resulting from a band-folding effect in the two-dimensional Brillouin zone of the in-plane wave vector ($k_\parallel$) of the Fe electrode. Since the in-plane cell size of $MgAl_2O_4$ is twice that of the primitive in-plane cell size of bcc Fe, the bands in the boundary edges are folded, and minority-spin states coupled with the Δ_1 evanescent state in the $MgAl_2O_4$ barrier appear at $k_\parallel = 0$, which reduces the TMR ratio of the MTJs significantly.

DOI: 10.1103/PhysRevB.86.024426 PACS number(s): 72.25.Mk, 73.40.Rw, 85.75.Dd

I. INTRODUCTION

Recent advances in tunneling magnetoresistance (TMR) in magnetic tunnel junctions (MTJs) with a single-crystal MgO barrier and bcc Fe ferromagnetic electrodes make possible the fabrication of ultrahigh-speed and high-density magnetic random access memory (MRAM) devices.[1–3] In Fe/MgO/Fe(001) MTJs, the crystal momentum parallel to the layer is conserved because of the two-dimensional (2D) periodicity of the system, and the tunneling conductance strongly depends on the symmetry of the propagating states in the bcc Fe electrode because of the complex band structures of MgO, which causes a slow decay of the evanescent Δ_1 state in the barrier layer. Furthermore, electrons with an in-plane wave vector $k_\parallel = (0,0)$ (normal incidence with respect to the plane) dominate the tunneling, and bcc Fe has a 100% spin polarization in the Δ_1 state at the Fermi level. Thus, Fe/MgO/Fe(001) MTJs act as spin filters for the current, yielding much larger TMR ratios of over 1000% in their ground state.[4,5]

Achieving a high TMR ratio in MgO-based MTJs requires epitaxial growth of the MgO layer with a correct crystalline orientation on ferromagnetic electrodes (bcc Fe and Co_xFe_{1-x}). However, it has been difficult to grow Fe/MgO/Fe(001) MTJs epitaxially due to the relatively large lattice mismatch (5%) between rock-salt-type MgO and bcc Fe. Recently, an off-stoichiometric, normal spinel $MgAl_2O_4$ barrier was grown epitaxially on a single-crystal $Co_2FeAl_{0.5}Si_{0.5}$ and bcc Fe to explore new materials for the barrier layer of MTJs.[6,7] Since normal spinel $MgAl_2O_4$ has a lattice constant a of 8.16 Å, the lattice mismatch with bcc-type ferromagnetic metals such as bcc Fe and Co-based full Heusler alloys is very small, i.e., less than 1% for a 45° (001) in-plane rotation, indicating that $MgAl_2O_4$ has the potential to overcome the problem associated with MgO barriers. In fact, a large room-temperature TMR ratio of over 100% was reported in $Co_2FeAl_{0.5}Si_{0.5}/MgAl_2O_4/CoFe(001)$ and $Fe/MgAl_2O_4/Fe(001)$ MTJs. Furthermore, a relatively large bias voltage for one-half the zero-bias TMR ratio was obtained at room temperature (RT), which is about twice that reported for MgO-based MTJs.

The band structures of bulk $MgAl_2O_4$ were investigated by first-principles density functional calculations,[8,9] and the results were compared with experimental data from vacuum ultraviolet measurements.[10] Normal spinel $MgAl_2O_4$ has an indirect band gap of about 7.8 eV (6.5 eV in calculations), and the Mg-O bond length (1.919 Å) is shorter than that in MgO (2.102 Å), implying a stronger bond and hence a larger band gap. However, the coherent tunneling properties of MTJs are still unknown for $MgAl_2O_4$. In particular, it is necessary to elucidate the symmetry-dependent tunneling through the evanescent states of $MgAl_2O_4$ and the physical cause of the relatively large TMR ratio obtained in recent experiments involving $Fe/MgAl_2O_4/Fe(001)$ MTJs.[7]

This work aims to determine the coherent tunneling properties of $MgAl_2O_4$ and the cause of the large TMR ratios in $Fe/MgAl_2O_4/Fe(001)$ MTJs. To this end, we investigated the spin-dependent transport properties of $Fe/MgAl_2O_4/Fe(001)$ MTJs on the basis of first-principles density functional calculations of the electronic structures and the ballistic conductance.

II. COMPUTATIONAL DETAILS

We prepared a supercell of a $Fe/MgAl_2O_4/Fe(001)$ MTJ containing 11 atomic layers of bcc Fe and 9 atomic layers of $MgAl_2O_4$. The in-plane lattice parameter of the supercell was fixed at 5.733 Å, which corresponds to twice the lattice constant of bcc Fe (2.865 Å). Since the lattice constant of spinel-type $MgAl_2O_2O$ is $a = 8.16$ Å, the lattice mismatch between bcc Fe and $MgAl_2O_4$ for a 45° (001) in-plane rotation is less than 1.0%. We performed first-principles calculations of the supercell using density functional theory within the generalized-gradient approximation for exchange-correlation energy.[11] To facilitate structure optimization, which is important for determining the interface structure, we adopted

plane-wave basis sets along with the ultrasoft pseudopotential method by using the quantum code ESPRESSO.[12] The number of **k** points was taken to be $5 \times 5 \times 1$ for all cases, and Methfessel-Paxton smearing with a broadening parameter of 0.01 Ry was used. The cutoff energies for the wave function and charge density were set to 30 and 300 Ry, respectively. These values are large enough to deal with all the elements considered here within the ultrasoft pseudopotential method.

For the conductance calculations, we considered an open quantum system consisting of a scattering region having a $MgAl_2O_4$ barrier and junctions with bcc Fe attached to left and right semi-infinite electrodes corresponding to bulk bcc Fe. The conductance was obtained by solving the scattering equation with infinite boundary conditions in which the wave function of the scattering region and its derivative were connected to the Bloch states of each electrode.[13] Since our system is repeated periodically in the xy plane and propagating states can be assigned by an in-plane wave vector $k_\parallel = (k_x, k_y)$ index, different $k_\parallel$ do not mix and can be treated separately. Furthermore, we neglected the spin-orbit interaction and noncollinear spin configuration. Thus, we solved the scattering equations for some fixed $k_\parallel$ and spin index on the basis of Choi and Ihm's approach.[13,14]

III. RESULTS AND DISCUSSION

First, we investigated the stable structure of $Fe/MgAl_2O_4(001)$ interfaces. Normal spinel $MgAl_2O_4$ has two different types of cation sites: tetrahedral Mg sites (A sites) and octahedral Al sites (B sites). This results in two types of termination for $Fe/MgAl_2O_4(001)$ junctions, namely, the A-site (Mg) termination and the B-site (Al-O) termination. On the basis of formation energy calculations for optimized surface structures of $MgAl_2O_4(001)$, we found that B-site termination is thermodynamically more stable than A-site termination. This was also reported for other normal spinel compounds, such as $Fe_3O_4(001)$.[15] Thus, we considered only B-site termination for the $Fe/MgAl_2O_4(001)$ interface. In B-site termination, there are four possible configurations, with the Fe atoms positioned on top of the Al atoms (Al-top), Al-Al hollow, Al-O hollow, and the O atoms (O-top) of $MgAl_2O_4$. We showed the top view of the $MgAl_2O_4(001)$ surface in Fig. 1(a) and corresponding Fe sites at the (001) face in Fig. 1(b). To determine the stable interfacial configuration at $Fe/MgAl_2O_4(001)$ junctions, we minimized the total energy by relaxing all atomic positions except for those in the electrode region by changing the longitudinal size of the supercell. Figures 1(c)–1(f) show schematics of the side view of the optimized $Fe/MgAl_2O_4/MgO(001)$ interfacial structures for each B-site termination. The total energies of each configuration relative to the O-top configuration are shown in Table I. We found that the O-top configuration is the most stable because of the hybridization between the $3d_{3z^2-r^2}$ orbital of Fe and the p_z orbital of O. Therefore, in the present study on spin-dependent conductance and the TMR effect, we adopted the O-top configuration for the B-site terminated $Fe/MgAl_2O_4(001)$ interface.

TABLE I. The total energies (ΔE_{total}) of each configuration relative to the O-top configuration in the B-site terminated $Fe/MgAl_2O_4(001)$ interface in eV/cell.

(eV/cell)	Al-top	Al-O hollow	Al-Al hollow	O-top
ΔE_{total}	1.60	1.55	2.85	0.00

Figure 2 shows the local density of states (LDOS) of Fe in $MgAl_2O_4/Fe(001)$, $MgO/Fe(001)$, and the bulk region. The interfacial LDOS of Fe at the interface with $MgAl_2O_4$ is modified from those in the bulk region due to the appearance of the nonbonding Fe-$3d_{x^2-y^2}$ and Fe-$3d_{xy}$ states around the Fermi level. The spin moment of interfacial Fe is $3.08\mu_B$,

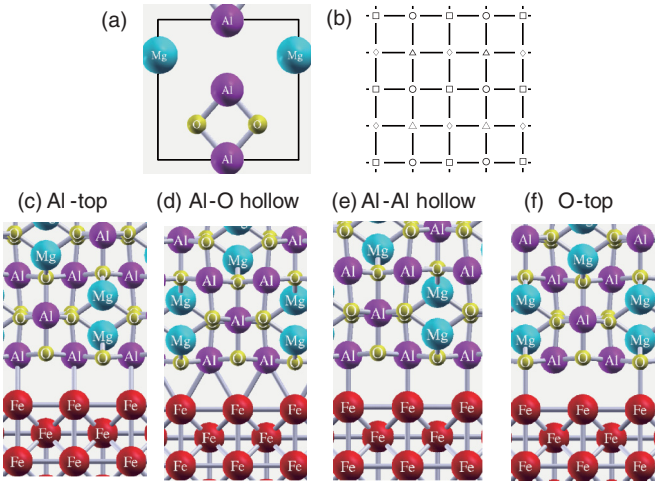

FIG. 1. (Color online) (a) Schematic figures of the top view of the $MgAl_2O_4(001)$ surface. (b) Corresponding Fe sites at the (001) face, where the square points, circle points, diamond points, and triangle points indicate Al-top, Al-O hollow, Al-Al hollow, and O-top configurations, respectively. The cross-sectional view is of a B-site terminated $Fe/MgAl_2O_4(001)$ interface with (c) Al-top, (d) Al-O hollow, (e) Al-Al hollow, and (f) O-top configurations.

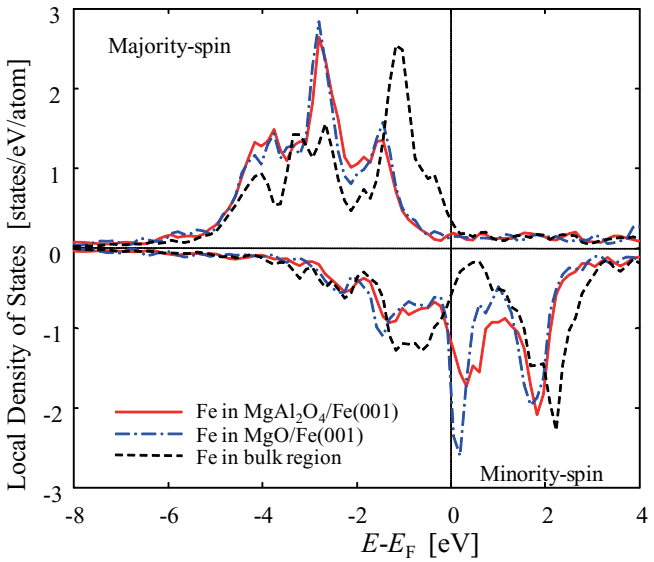

FIG. 2. (Color online) Local density of states (LDOS) of interfacial Fe at $MgAl_2O_4/Fe(001)$ and $MgO/Fe(001)$ interfaces together with bulk Fe as a function of energy relative to the Fermi energy.

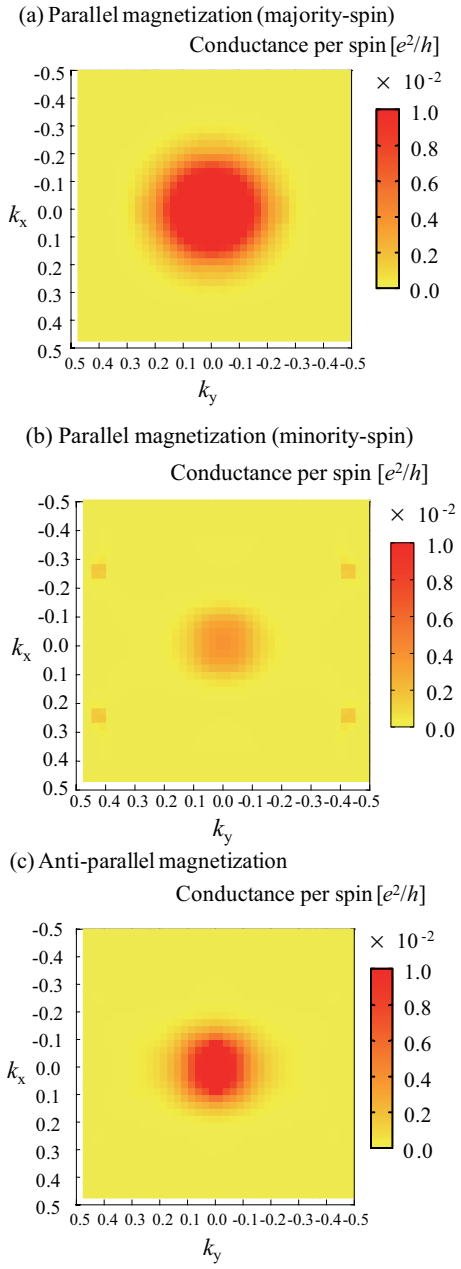

FIG. 3. (Color online) In-plane wave vector $k_\parallel = (k_x,k_y)$ dependence of (a) majority- and (b) minority-spin conductance at the Fermi level for $Fe/MgAl_2O_4/Fe(001)$ MTJs with parallel magnetization and (c) antiparallel magnetization.

which is larger than that in the bulk region ($2.49\mu_B$). Similar results have been obtained for MgO/Fe(001) interfaces.[4,16]

We investigated the tunneling conductance of the $Fe/MgAl_2O_4(\sim 1$ nm)/Fe(001) MTJ. Figure 3 plots the in-plane wave vector ($k_\parallel$) dependence of the tunneling conductance at the Fermi level for the $Fe/MgAl_2O_4/Fe(001)$ MTJ in parallel and antiparallel magnetization configurations. We confirmed in Fig. 3(a) that the majority-spin conductance for the parallel magnetization has a broad peak around the center of the 2D Brillouin zone. This is the typical behavior of the coherent tunneling conductance of Δ_1 electrons at $k_\parallel = (0,0)$. Furthermore, we found in Fig. 3(b) that the minority-spin conductance for the parallel magnetization also shows a broad peak at $k_\parallel = (0,0)$. This result is very different from that for the Fe/MgO/Fe(001) MTJ,[4,5] where the $k_\parallel$ dependence of the minority-spin conductance for the parallel magnetization shows hotspot-like peaked structures in the 2D Brillouin zone with no peak at $k_\parallel = (0,0)$ because of the absence of the Δ_1 band around the Fermi level. Since the tunneling conductance in the antiparallel magnetization shows a combination of the features observed in the majority and minority spin channels, we obtained a broad peak at $k_\parallel = (0,0)$ in the $k_\parallel$ dependence of the conductance for the antiparallel magnetization as shown in Fig. 3(c). In Table II, we showed the majority- and minority-spin conductance and the TMR ratios for $Fe/MgAl_2O_4/Fe(001)$ MTJs and Fe/MgO/Fe(001) MTJs. The calculated minority-spin conductance for the $Fe/MgAl_2O_4/Fe(001)$ MTJ for parallel magnetization was one order of magnitude higher than that for the Fe/MgO/Fe(001) MTJ. This led to a TMR ratio of 160% for the $Fe/MgAl_2O_4/Fe(001)$ MTJ, which was much lower than that for the Fe/MgO/Fe(001) MTJ (1600%) with the same barrier thickness.

Figure 4 shows the imaginary part of the out-of-plane wave vector k_z (κ) at the Fermi levels of bulk $MgAl_2O_4$ and MgO as a function of the in-plane wave vector k_x. The positions of the Fermi level in the band gap were determined from the LDOS of oxygen atoms in the center of the barrier layer of $Fe/MgAl_2O_4/Fe(001)$ and Fe/MgO/Fe(001) MTJs. Since propagating states in the metal electrode couple to evanescent states (κ) in the barrier layer and decay as $\sim e^{-\kappa z}$, the evanescent state with the smallest decay parameter, $\kappa_{\min}$, makes the largest contribution to the tunneling conductance in MTJs. We found that at $(k_x,k_y) = (0,0)$, $MgAl_2O_4$ has the smallest κ with Δ_1 symmetry in the gap connecting the top of the Δ_1 valence band to the bottom of the Δ_1 conduction band, which is similar to the case for rock-salt-type MgO. This could be due to the hybridization between O $2p_z$ and Mg $2p_z$, generating the energy gap along the Δ line. Furthermore, the lowest κ of $MgAl_2O_4$ showed a k_x dependence similar to that for MgO. This suggests the possibility that the large TMR ratio stems from the coherent tunneling properties and the half-metallic character of bcc Fe on the Δ_1 state in $Fe/MgAl_2O_4/Fe(001)$, as in Fe/MgO/Fe(001) MTJs. These results are inconsistent with our calculation results, where the TMR ratio of the $Fe/MgAl_2O_4/Fe(001)$ MTJ (160%) was one order of magnitude smaller than that of the Fe/MgO/Fe(001) MTJ (1600%).

To further elucidate these results, we show in Fig. 5 the band dispersion of bulk bcc Fe with a tetragonal unit cell ($a = 5.733$ Å, $c/a = 0.5$), corresponding to the unit cell of the electrode region in the $Fe/MgAl_2O_4/Fe(001)$ MTJ. Since bcc Fe with a primitive lattice constant of 2.867 Å has minority-spin states with s orbital character at the boundary edge of the 2D Brillouin zone of $k_\parallel$, these minority-spin states appear at $k_\parallel = (0,0)$ because of the band folding that occurs when the in-plane cell size of bcc Fe is twice that of the primitive cell size. The new conductive channels at $k_\parallel = (0,0)$ couple with the Δ_1 evanescent states of $MgAl_2O_4$, giving the slowest decay in the barrier layer. This induces a relatively large conductance in the antiparallel magnetization configuration, resulting in the reduction of the TMR ratio. Thus, we concluded that the TMR

TABLE II. Calculated majority-spin and minority-spin conductance for parallel and antiparallel magnetization and TMR ratios for $Fe/MgAl_2O_4/Fe(001)$ and Fe/MgO/Fe(001) MTJs with the same barrier thickness (∼1.2 nm).

	Conductance ($S/\mu m^2$)				
	Parallel magnetization		Antiparallel magnetization		
	Majority spin	Minority spin	Majority spin	Minority spin	TMR ratio (%)
$Fe/MgAl_2O_4/Fe(001)$ MTJ	0.5	0.02	0.1	0.1	160
Fe/MgO/Fe(001) MTJ	0.1	0.003	0.003	0.003	1600

effect in $Fe/MgAl_2O_4/Fe(001)$ MTJs is intrinsically smaller than that of Fe/MgO/Fe(001) MTJs because of the band folding effect in the minority-spin states of the Fe electrode.

Of course, the new folded minority-spin channel having s-character always appears in the Fe electrodes at $k_\parallel = (0,0)$ if we suppose a doubled in-plane unit cell geometry in the Fe/MgO/Fe(001). However, in this case, the Brillouin zone folding occurs also in the MgO. Thus, the folded minority-spin Fe-s channels are coded as the different $k_\parallel$ compared with the unfolded states, and they are connected to the new folded evanescent states of MgO at $k_\parallel = (0,0)$, showing the fast decay in the MgO region, which is the same situation as that with the primitive unit cell. On the other hand, in the case of the $Fe/MgAl_2O_4/Fe(001)$, there are no folded states in the $MgAl_2O_4$. In this case, the folded minority-spin Fe-s channels at $k_\parallel = (0,0)$ have the total symmetry in the unit cell of the $Fe/MgAl_2O_4/Fe(001)$, and they are connected to the Δ_1 evanescent states in the $MgAl_2O_4$.

Then, we calculated the projection of the scattering wave function on the local atomic orbital of the MTJs at the Fermi level ($|c_{\alpha lm}|^2$). Here, the α, l, and m are indices of atom positions and local atomic orbitals, and the formulation of the $|c_{\alpha lm}|^2$ was given in Ref. 13. Figure 6 presents the $|c_{\alpha lm}|^2$ of oxygen atoms for the majority-spin and the minority-spin states at $k_\parallel = (0,0)$ as a function of the distance from the left junction of the $Fe/MgAl_2O_4/Fe(001)$ and Fe/MgO/Fe(001) MTJs in parallel magnetization. Note that the tetragonal distortion of the $MgAl_2O_4$ causes the relaxation of oxygen atoms in the unit cell, making the different O atoms at the same (001) plane of the $MgAl_2O_4$. We found that the MTJ with the $MgAl_2O_4$ has the slow decay evanescent states originating from the Fe-s channels both in the majority- and minority-spin states, leading to the reduction of the TMR ratio. On the other hand, the MTJ with the MgO has the slow decay states only in the majority-spin states. The folded minority-spin s-channel clearly shows a fast decay in the MgO barrier compared with that in the $MgAl_2O_4$.

Furthermore, we found that the $|c_{\alpha(\Delta_1)}|^2$ of interfacial O atoms in the minority-spin states is much smaller than that of the majority-spin states. This means that the overlap of the scattering wave function of the Δ_1 states between Fe and $MgAl_2O_4$ reduces in the minority-spin channel compared with the majority-spin channel. This is the reason why we obtained the TMR ratio over 100% in spite of the non-half-metallic behavior of the Δ_1 states in the $Fe/MgAl_2O_4/Fe(001)$ MTJs.

It is also found that the $|c_{\alpha(\Delta_1)}|^2$ of the $Fe/MgAl_2O_4/Fe(001)$ MTJ showed a slower decay for the wave function of the Δ_1 evanescent state than for the Δ_5 state. The same was observed in the case of the Fe/MgO/Fe(001) MTJ. This is clear evidence of the significant contribution of tunneling electrons with Δ_1 symmetry, as compared to those with Δ_5 symmetry in $MgAl_2O_4$. Furthermore, the decay rate of the $|c_{\alpha(\Delta_1)}|^2$ in the interior of the barrier layer is almost the same for both $Fe/MgAl_2O_4/Fe(001)$ and Fe/MgO/Fe(001) MTJs. These results indicate that MTJs with a $MgAl_2O_4$ barrier can potentially show a large TMR ratio, comparable to that for Fe/MgO/Fe(001) MTJs, if band folding of the Fe electrode can be suppressed.

Finally, we discuss a possibility of the coherent tunneling and the band folding in recent experiments of MTJs with

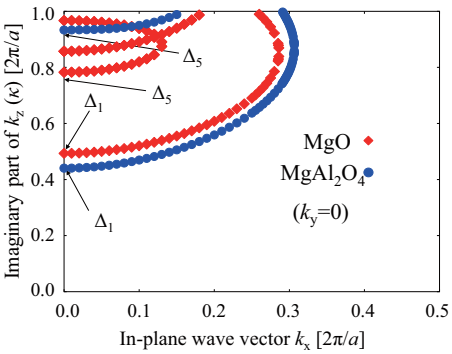

FIG. 4. (Color online) Imaginary part of k_z as a function of real k_x at the Fermi levels for bulk MgO and $MgAl_2O_4$. Note that the Fermi levels for bulk MgO and $MgAl_2O_4$ are determined from the LDOS of oxygen atoms in the center of the insulating layer of each MTJ.

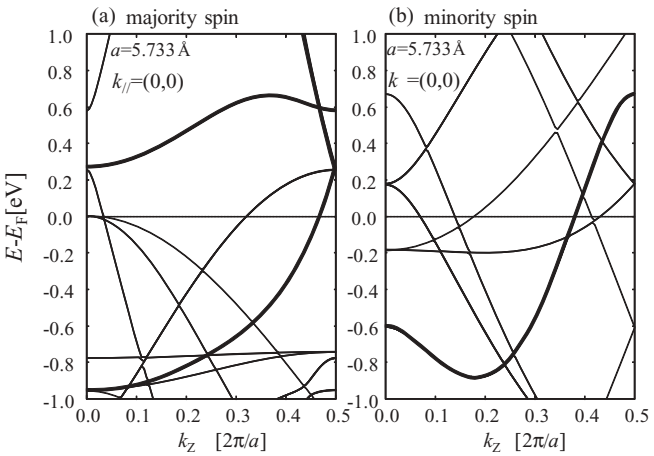

FIG. 5. (a) Majority- and (b) minority-spin band dispersion of the bcc Fe electrode in $Fe/MgAl_2O_4/Fe$ MTJs with a tetragonal unit cell ($a = 5.733$ Å, $c/a = 0.5$) along the [001] direction at $k_\parallel = (0,0)$, where the bold lines indicate the band with Δ_1 symmetry in the tetragonal unit cell, which corresponds to the unit cell of $MgAl_2O_4$.

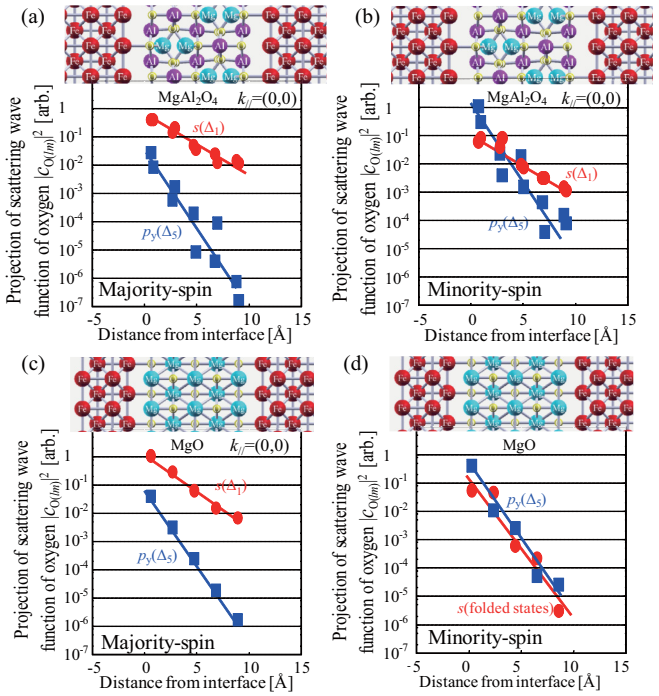

FIG. 6. (Color online) The projection of the scattering wave function on the $\Delta_1(s)$ and $\Delta_5(p_y)$, and folded s states of oxygen atoms at the Fermi level as a function of the distance from the left interface for a normal junction of (a) the majority-spin states in $Fe/MgAl_2O_4(001)$, (b) the minority-spin states in $Fe/MgAl_2O_4(001)$, (c) the majority-spin states in Fe/MgO(001), and (d) the minority-spin states in Fe/MgO(001). The scale of the vertical axis is logarithmic. The solid lines are guides to the eye

the $MgAl_2O_4$ barrier. Sukegawa *et al.* reported TMR ratios of 117% at RT and 165% at 15 K for $Fe/MgAl_2O_x$(1.0–1.5 nm)/Fe(001) MTJs.[7] They showed that the $MgAl_2O_x$ barrier layer formed a normal-spinel structure with a (001) orientation, and the $Fe/MgAl_2O_x/Fe(001)$ MTJ had an epitaxial relationship between the bcc-Fe(001)[110] and the $MgAl_2O_x(001)$. This means that the coherent tunneling occurs through the evanescent Δ_1 state in the barrier layer. Thus, the experimentally observed small TMR ratio in the $Fe/MgAl_2O_x/Fe(001)$ MTJ compared to that of the Fe/MgO/Fe(001) MTJ (Refs. 1–3) can be attributed to the appearance of new conductive channels in the antiparallel magnetization due to the band folding effect. We believe that a modification of the periodic boundary condition along the in-plane direction by choosing ferromagnetic electrodes without the band folding at the junction with $MgAl_2O_4$, i.e., the ferromagnetic metals having the lattice constant corresponding to the $MgAl_2O_4$ or the half-metallic ferromagnets, is necessary to obtain the large TMR ratio in MTJs with the normal-spinel $MgAl_2O_4$.

IV. SUMMARY

We investigated the electronic and transport properties of $Fe/MgAl_2O_4/Fe(001)$ MTJs on the basis of first-principles density functional calculations. Since normal spinel $MgAl_2O_4$ has evanescent states with Δ_1 symmetry in the energy gap around the Fermi level, the $Fe/MgAl_2O_4/Fe(001)$ MTJ, like Fe/MgO/Fe(001), shows coherent tunneling properties. However, we obtained a TMR ratio of 160% for the $Fe/MgAl_2O_4$(1 nm)/Fe(001) MTJ, which was much smaller than that of the Fe/MgO(1 nm)/Fe(001) MTJ (1600%). We concluded that the appearance of new conductive channels at $k_\parallel = (0,0)$ due to the band folding effect significantly reduced the TMR ratio of the $Fe/MgAl_2O_4$(1 nm)/Fe(001) MTJ. The new folded channel in the minority-spin state of the Fe electrode coupled with the Δ_1 evanescent state of the $MgAl_2O_4$ barrier, which showed a slow decay in the barrier layer and contributed to the minority-spin conductance. These results indicate that the TMR effect in $Fe/MgAl_2O_4/Fe(001)$ MTJs is intrinsically smaller than that in Fe/MgO/Fe(001) MTJs. However, if the band folding effect can be suppressed by changing the periodic boundary condition along the in-plane direction, e.g., the ferromagnetic metals having the lattice constant corresponding to the $MgAl_2O_4$ or the half-metallic ferromagnets, the $Fe/MgAl_2O_4/Fe(001)$ MTJs show a large TMR ratio, comparable to that for Fe/MgO/Fe(001) MTJs.

ACKNOWLEDGMENTS

We are grateful to H. Sukegawa and S. Mitani of the National Institute for Materials Science in Japan for valuable discussions about our work. This work was supported by a Grant-in-Aid for Scientific Research (No. 22360014 and No. 22760003) from MEXT, the Japan Science and Technology (JST) through its Strategic International Cooperative Program under the title "Advanced spintronic materials and transport phenomena (ASPIMATT)." Y.M. and K.A. gratefully acknowledge support from the Mayekawa Houonkai Foundation.

*miura@riec.tohoku.ac.jp

[1] S. Yuasa, T. Nagahama, A. Fukushima, Y. Suzuki, and K. Ando, Nat. Mater. **3**, 868 (2004).
[2] S. S. P. Parkin, C. Kaiser, A. Panchula, P. M. Rice, B. Hughes, M. Samant, and S.-H. Yang, Nat. Mater. **3**, 862 (2004).
[3] S. Ikeda, J. Hayakawa, Y. M. Lee, F. Matsukura, Y. Ohno, T. Hanyu, and H. Ohno, IEEE Trans. Electron Devices **54**, 991 (2007).
[4] W. H. Butler, X.-G. Zhang, T. C. Schulthess, and J. M. MacLaren, Phys. Rev. B **63**, 054416 (2001).
[5] J. Mathon and A. Umerski, Phys. Rev. B **63**, 220403(R) (2001).
[6] R. Shan, H. Sukegawa, W. H. Wang, M. Kodzuka, T. Furubayashi, T. Ohkubo, S. Mitani, K. Inomata, and K. Hono, Phys. Rev. Lett. **102**, 246601 (2009).
[7] H. Sukegawa, H. Xiu, T. Ohkubo, T. Furubayashi, T. Niizeki, W. Wang, S. Kasai, S. Mitani, K. Inomata, and K. Hono, Appl. Phys. Lett. **96**, 212505 (2010).
[8] Y.-N. Xu and W. Y. Ching, Phys. Rev. B **43**, 4461 (1991).

[9]R. Khenata, M. Sahnoun, H. Baltache, M. Rerat, A. H. Reshak, Y. Al-Douri, and B. Bouhafs, Phys. Lett. A **344**, 271 (2005).
[10]M. L. Boltz, R. H. French, D. J. Jones, R. V. Kasowski, and F. S. Phuchi, Phys. Scr. **41**, 4404 (1990).
[11]J. P. Perdew, K. Burke, and M. Ernzerhof, Phys. Rev. Lett. **77**, 3865 (1996).
[12]S. Baroni, A. Dal Corso, S. de Gironcoli, and P. Giannozzi, http://www.pwscf.org.
[13]H. J. Choi and J. Ihm, Phys. Rev. B **59**, 2267 (1999).
[14]A. Smogunov, A. Dal Corso, and E. Tosatti, Phys. Rev. B **70**, 045417 (2004).
[15]M. Fonin, R. Pentcheva, Yu. S. Dedkov, M. Sperlich, D. V. Vyalikh, M. Scheffler, U. Rüdiger, and G. Güntherodt, Phys. Rev. B **72**, 104436 (2005).
[16]T. Saito, T. Katayama, T. Ishikawa, M. Yamamoto, D. Asakura, T. Koide, Y. Miura, and M. Shirai, Phys. Rev. B **81**, 144417 (2010).